Journal of Sound and Vibration (2003) **259**(5), 1147–1161
doi:10.1006/jsvi.2002.5190, available online at http://www.idealibrary.com on IDEAL®

STUDY OF THE IMPULSE WAVE DISCHARGED FROM THE EXIT OF A RIGHT-ANGLE PIPE BEND

H.-D. Kim

School of Mechanical Engineering, Andong National University, 388 *Songchun-dong, Andong* 760-749*, South Korea. E-mail: kimhd@andong.ac.kr*

D.-H. Lee

Department of Mechanical Engineering, Seoul National University of Technology, 172*, Kongneung-dong, Nowon* 139-743*, South Korea*

AND

T. Setoguchi

Department of Mechanical Engineering, Saga University, 1 *Honjo-machi, Saga-shi, Saga* 840-8502*, Japan*

(*Received* 1 *July* 2001, *and in final form* 30 *April* 2002)

The impulse wave, which is usually generated by a shock wave discharge from the exit of a pipe, almost always leads to undesirable noise and vibration problems. The present study addresses experimental and computational work of the impulse wave discharged from the exit of two kinds of right-angle pipe bends, which are attached to the open end of a simple shock tube. The weak normal shock wave with its magnitude of Mach number from 1·02 to 1·20 is employed to obtain the impulse wave propagating outside the exit of the pipe bends. A Schlieren optical system is employed to visualize the impulse wave discharged from the exit of the pipe bends at an instant. The experimental data of the magnitude of the impulse wave and its propagation directivity are analyzed to characterize the impulse waves discharged from the exit of the pipe bends and compared with those discharged from a straight pipe. Computational analysis using the unsteady, inviscid, compressible equations is complemented to represent the major features of the impulse wave obtained from the shock tube experiments. Computational results well predict the experimented dynamic behaviors of the impulse wave. The results obtained show that a right-angle miter bend considerably reduces the magnitude of the impulse wave and its directivity toward to the pipe axis, compared with the straight pipe. It is believed that the right-angle miter bend pipe can play one role of a passive control against the impulse wave.

1. INTRODUCTION

A sudden discharge of mass flow from the exit of a pipe often gives rise to an impulse wave propagating into the surroundings. The impulse wave is generally characterized by a high peak pressure of short duration [1], and usually leads to severe noise and vibration problems. To understand the characteristics of the impulse wave and thereby to find a proper control strategy, it is of practical importance to investigate the time-dependent dynamic behaviors of the impulse wave.

The impulse wave has been investigated so far using a simple shock tube with an open end. The major characteristics of the impulse waves, which are produced in the exit of a

0022-460X/02/$35.00

straight pipe, are well understood; the peak pressure and directivity of the impulse wave are a function of Mach number of the initial normal shock wave inside a pipe [2, 3] Recently, Kim *et al.* [4] showed some possibilities to control the impulse wave by changing the configuration of the pipe exit. They also investigated the impingement of the impulse wave upon a flat plate and showed a good empirical equation to predict the peak pressure of the impulse wave formed on the plate surface [5]. Almost all of these work which have been conducted to date are limited to the impulse wave discharged from the exit of a straight pipe.

There are, however, many industrial and engineering applications, in which the impulse waves occur at the exit of pipe bends, such as internal combustion engine exhaust mufflers [6, 7], high-pressure gas blow-off systems [8], pulse jet system [9], etc. In these cases, the characteristics of the impulse wave discharged from the exit of the pipe bend may be different from those of the straight pipe. The impulse wave can be related to shock wave reflection and diffraction phenomena occurring in the process of propagation through the bend. Even for the initial normal shock wave given at the pipe inlet, the shock structure at the exit of the pipe bend would be highly distorted when the normal shock wave passes through the bend.

Dynamic behaviors of the shock wave propagating through a pipe bend have been well understood; some works [10, 11] have addressed the major features of the shock reflection and diffraction occurring in the pipe bend. Recently, Sarigül [12] made use of Helmholtz integral equation to investigate the sound attenuation characteristics of an acoustic wave propagating through a right-angle pipe bend and showed that sharper bend provides more sound attenuation corresponding to higher wave numbers in a wider range. He also argued that bending a pipe at a right angle with a sharpness r/R less than 0·5 would not provide a considerable sound attenuation, where r and R mean the pipe radius and the median arc radius of the pipe bend respectively. This work has motivated the present study to investigate the impulse wave discharged from the exit of a right-angle pipe bend.

The present study describes experimental and computational works to understand the impulse wave discharged from the exit of two different kinds of right-angle pipe bends. The impulse wave is made by a weak shock wave discharge from the open end of the pipe bends. The pipe bends are attached to the low-pressure chamber of a simple shock tube with an open end. The discharged impulse wave is characterized by static pressure measurements at the exterior of the pipe bends. A Schlieren optical system enables the impulsive wave to visualize at a certain instant. Computational analysis is carried out to detail the impulse wave obtained from experiments and the wave structures inside the bend, not being able to visualize them in experiment. Two-dimensional, unsteady, inviscid, compressible equations are solved numerically using the Harten–Yee TVD scheme [13]. The second-order total variation diminishing (TVD) is incorporated into an operator splitting technique [14]. The results obtained show that a right-angle miter bend considerably reduces the magnitude of the impulse wave and its directivity toward the pipe axis, compared with the straight pipe.

2. EXPERIMENTAL FACILITIES AND MEASUREMENT

The simple open-ended shock tube has a diameter (D) of 66 mm and a total length of about 3·765 m (the length of the driven section: 2·145 m), as shown in Figure 1. A sheet of cellophane with 0·03 mm thickness is used as a diaphragm, which is manually ruptured to initiate the shock wave motion. The initial pressure ratio of the shock tube is set to obtain

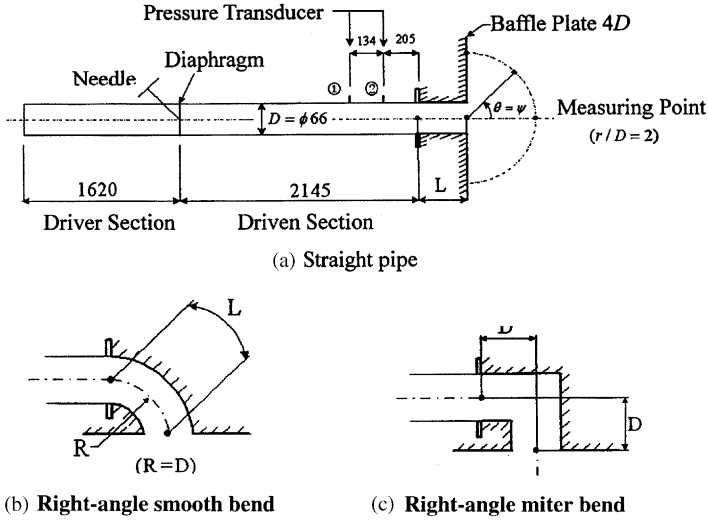

Figure 1. Experimental apparatus and right-angle pipe bends.

shock Mach number, M, below 1·20, the driven air being initially at atmospheric pressure and room temperature.

A straight pipe of diameter D is connected to the open end of the shock tube and has its length L (= 104 mm), as shown in Figure 1. Two kinds of pipe bends, as also schematically shown in Figure 1, are attached to the open end of the shock tube so that the impulse wave can be produced by the discharge of shock wave from the exit of the pipe bends. A right-angle smooth bend has the median arc radius of R $(= D)$, and its median length is L $(= 2D)$. A right-angle miter bend, as also shown in Figure 1(c), has the median length of $2D$.

To characterize the impulse wave discharged from the exit of these bends, Figure 2 shows the Cartesian co-ordinate system employed in the present study. For reference, θ is defined as an angle to the x-axis on the x–y plane and ψ an angle to the x-axis on x–z plane.

A baffle plate of diameter of $4D$ is installed at the exit of the bends to be free from the pipe end effects which may occur at the exit of the bends [15, 16]. The initial pressures of the shock tube are monitored by a personal computer system. Calibrated pressure transducers (PCB112A21), flush mounted on the shock tube walls at several stations, are used to measure and characterize the shock wave propagating through the tube. In particular, static pressures at the positions of 339 mm (the measuring point ②) and 205 mm (the measuring point ①) from the exit of the shock tube are employed to establish the shock Mach number M.

Another pressure transducer (PCB112A21) is flush mounted on a small wedge probe to measure the static pressures of the impulse wave at a certain location. In the present study, the static pressure measurements of the impulse wave are mainly carried out at $r/D = 2{\cdot}0$, where r means the distance from the exit of the pipe bend, as also shown in Figure 1. On the baffle plate, the pressure signals from a transducer trigger the Schlieren optical system for visualization of the impulse wave. The Schlieren system is incorporated into a delay circuit so that it allows the visualization of the impulse wave structure discharging from the exit of the bends at an instant. The light source for the Schlieren

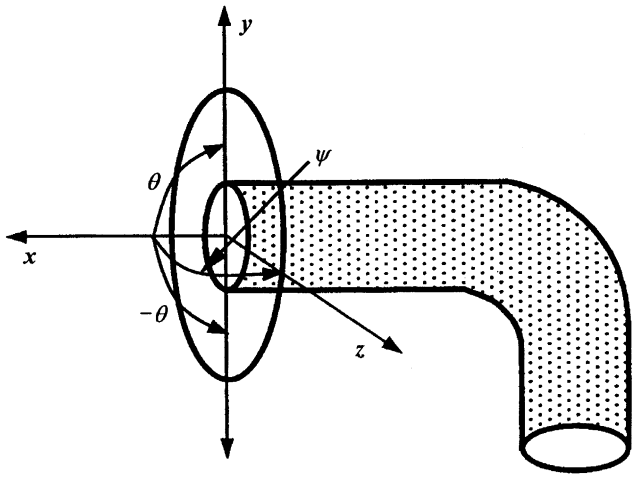

Figure 2. Co-ordinate system for pressure measurement.

system is provided by Mg strobrite spark lamp. The duration of the light flash is about 1 μs. Output of the pressure transducer is recorded on an X–Y recorder by way of a wave memory. The pressure transducers were calibrated both statically and dynamically prior to each test. The uncertainty in pressure measurements is estimated to be less than ±1·5%. These estimations are based on the maximum possible fluctuations in the measurements.

3. COMPUTATIONAL ANALYSIS

The impulse wave discharged from the open end of the pipe bend is simulated using a computational fluid dynamics (CFD) method. Two-dimensional, unsteady, inviscid, conservation equations are solved numerically by assuming a perfect gas ($\gamma = 1{\cdot}4$),

$$\frac{\partial U}{\partial t} + \frac{\partial F}{\partial x} + \frac{\partial G}{\partial y} + H = 0, \tag{1}$$

$$U = \begin{bmatrix} \rho \\ \rho u \\ \rho v \\ e \end{bmatrix}, \quad F = \begin{bmatrix} \rho u \\ \rho u^2 + p \\ \rho uv \\ (e+p)u \end{bmatrix}, \quad G = \begin{bmatrix} \rho v \\ \rho uv \\ \rho v^2 + p \\ (e+p)v \end{bmatrix}, \quad H = \frac{1}{y}\begin{bmatrix} \rho v \\ \rho uv \\ \rho v^2 \\ (e+p)v \end{bmatrix},$$

where x and y are the Cartesian co-ordinates, t the time, ρ the density and, u and v are the velocity components for x and y directions respectively. The total energy e per unit volume of the gas is expressed by the sum of the kinetic energy and the internal energy as follows:

$$e = \frac{p}{\gamma - 1} + \rho\left(\frac{u^2 + v^2}{2}\right). \tag{2}$$

Equation (1) is closed by the thermal equation of state of a perfect gas, $p = \rho RT$, where T is the temperature. In the computations, equation (1) is rewritten in a non-dimensional form by referring the quantities, the pressure, density, etc. to atmospheric conditions and

the diameter of the shock tube.

$$x' = \frac{x}{D}, \quad y' = \frac{y}{D}, \quad u' = \frac{u}{a_a/\sqrt{\gamma}}, \quad v' = \frac{v}{a_a/\sqrt{\gamma}},$$

$$t' = \frac{t}{\sqrt{\gamma}D/a_a}, \quad p' = \frac{p}{p_a}, \quad \rho' = \frac{\rho}{\rho_a}, \quad e' = \frac{e}{p_a}. \tag{3}$$

The superscript ($'$) indicating the non-dimensional quantities is omitted for the sake of simplicity. The subscript **a** denotes atmospheric state ahead of the shock wave. For instance, $\mathbf{a}_a$ means the speed of sound at the atmospheric conditions. The resulting nondimensional form of equation (1) is solved numerically using the Harten–Yee TVD scheme [13]. The second order TVD is incorporated into the operator splitting technique which was suggested by Sod [14].

The fineness of computational grid required to obtain grid independent solutions was first examined for some of the impulse waves discharged from the exit of the shock tube. The grid density over $\Delta x = \Delta y = 70/D$ seemed to change the accuracy of obtained solutions no longer. A grid size of $\Delta x = \Delta y = 75/D$ is employed in the present computations which ensure that the solutions obtained were independent of the grid density.

4. RESULTS AND DISCUSSION

Figure 3 shows the experimented pressure histories of the impulse wave on x–y plane at the exit of the straight pipe. At $\theta = 0^\circ$, the impulse wave seems to have a very short rising time and high peak value. After the peak value, the pressure suddenly drops down and

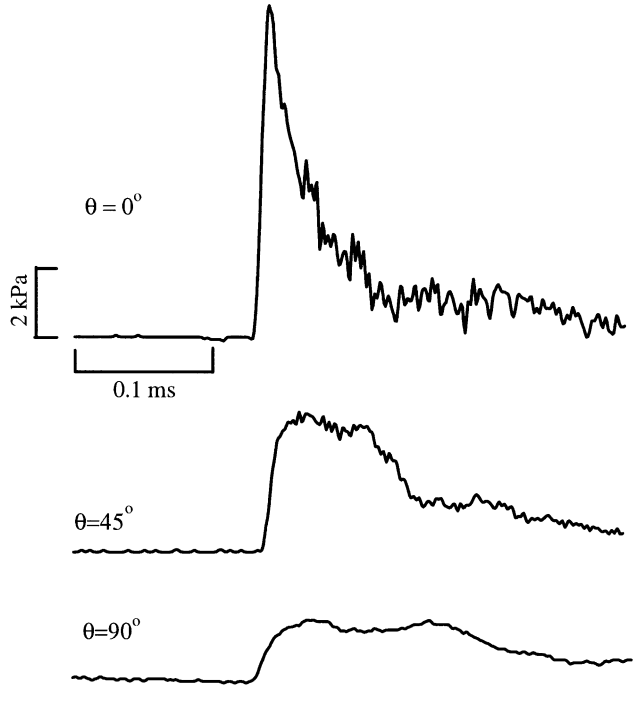

Figure 3. Pressure signals of the impulse wave at the exit of the straight pipe ($M = 1{\cdot}10$).

then fluctuates due to the flow just behind the impulse wave and partly due to the wave reflection and diffraction on the wedge probe for installation of the pressure transducer. From the pressure signals of the measurement points ① and ② the Mach number, M, of the initial shock wave is calculated by 1·10. At $\theta = 0°$, the impulse wave is quite different from that at $\theta = 45$ and 90°; the peak pressure is much higher than that at $\theta = 45$ and 90°, and the rising time to the peak value seems much shorter. At $\theta = 90°$, there is no discrete peak value and the pressure fluctuations seem to be much smaller than those at $\theta = 0°$. This implies that the impulse wave on the pipe axis should be stronger than that at $\theta = 45$ and 90°.

For the same Mach number of $M = 1{\cdot}10$, Figure 4 shows the measured pressure signals at the exit of the right-angle smooth bend. The dependency of the impulse wave on θ seems to be a little different from that of the straight pipe, as shown in Figure 3. For instance at $\theta = 0°$, the impulse wave has a sharp peak after an initially gradual rise in pressure. At $\theta = 45$ and 90°, the pressure signals are different from those at $\theta = 0°$; there is no appreciable pressure rise before the sharp peak value. The pressure transducer on the wedge probe at $\theta = 0°$ seems to detect the pressure signals earlier than those at $\theta = 45$ and 90°. The propagation speed of the impulse wave at $\theta = 0°$ seems faster than that at $\theta = 45$ and 90°. However, it is found that the propagation speeds of the impulse wave for different ψ are nearly the same, as shown in Figure 5. At both directions of $\psi = 0°$ and

Figure 4. Pressure signals of the impulse wave at the exit of the right-angle smooth bend ($M = 1{\cdot}10$).

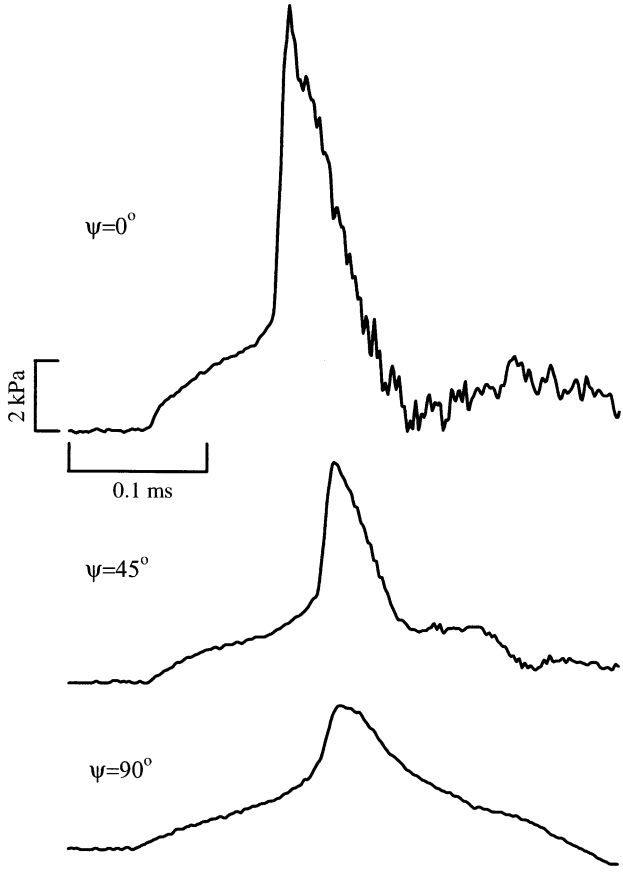

Figure 5. Pressure signals of the impulse wave at the exit of the right-angle smooth bend ($M = 1{\cdot}10$).

$\theta = 0^\circ$, the magnitudes of the impulse wave are stronger than those at different angles of ψ and θ. It is interesting to note that the impulse wave formed at the exit of the right-angle smooth bend has a small pressure rise before the sharp peak value, as shown at $\psi = 0^\circ$ and $\theta = 0^\circ$.

Figure 6 shows the pressure signals measured at the exit of the right-angle miter bend at the same Mach number of $M = 1{\cdot}10$. The impulse wave at θ direction has a sharp pressure rise, unlike that at the exit of the right-angle smooth bend. There are some peak values in the pressure signals and after the peaks, the pressure highly fluctuates due to the discharge of the reflected waves from the miter bend, as will be described later.

Figure 7 shows the pressure signals at the measurement points ① and ② inside the shock tube. At both the straight pipe and right-angle smooth bend, the pressure signals at the measurement points ① and ② show a very steep pressure rise due to the incident shock wave and then remain constant before a sudden drop due to the expansion waves reflected from the exit of the pipe. Unlike the pressure signals at the right-angle smooth bend, it is found that at the right-angle miter bend the pressure steeply rises again, after the sudden pressure rise due to the incident shock wave, as indicated by A and B; the second pressure rise is due to the shock wave reflected from the downstream wall of the miter bend. The reflected shock waves would be again reflected from the contact surface or the diaphragm and then discharged to produce the impulse waves, which are shown in Figure 6.

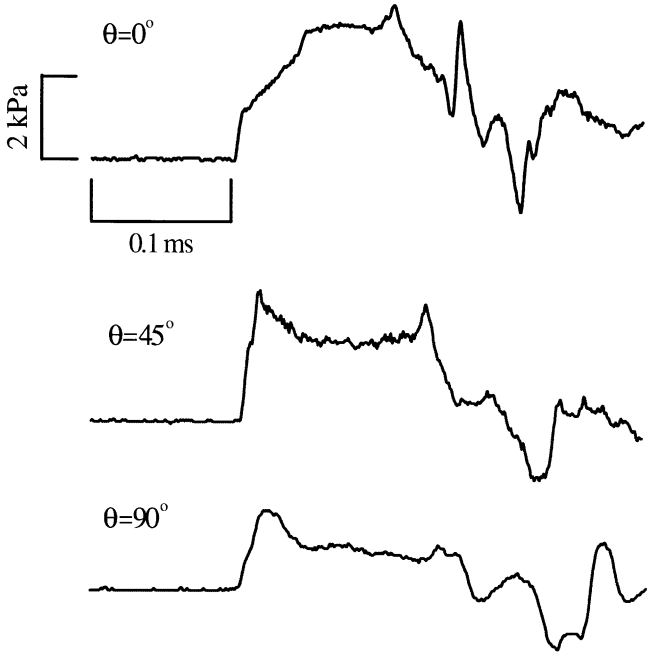

Figure 6. Pressure signals of the impulse wave at the exit of the right-angle miter bend ($M = 1{\cdot}10$).

Figure 8 shows the Schlieren picture and computed density contours of the impulse wave discharged from the exit of the straight pipe. Note that the Schlieren picture was taken at the delay time of 50 μs after the impulse wave passes over the pressure transducer on the baffle plate, which is schematically shown in Figure 8, while the computational result was obtained at a non-dimensional time $t' = 1{\cdot}6959$, corresponding to nearly the same instant that the experimented impulse wave is discharged from the exit of the straight pipe. The impulse wave is of a cylindrical and symmetrical form and its magnitude seems to be stronger on the pipe axis. It is also found that the computed density contours obtained from the present computation predicts the experimented impulse wave well.

For both the bends, Figures 9 and 10 show the Schlieren picture and the computed density contours of the impulse wave at Mach number of 1·10. Note again that both the experimented and computed impulse waves are not for exactly the same time. The impulse wave discharged from the exit of the bends is neither symmetrical nor cylindrical. Compared with that of the straight pipe, it seems to be weaker in its magnitude and to be highly deviated toward the bend. This is due to the shock wave reflection and diffraction inside the bend.

Both the reflected shock wave and impulse wave are found in the computed density contour for the right-angle miter bend, as seen in Figure 10. Some part of the initial normal shock wave reflects from the downstream wall of the right-angle miter bend and the resulting shock wave is seen inside the bend. The other part of the initial normal shock wave is discharged from the exit of the bend to produce an impulse wave. However, for the right-angle smooth bend, the reflected shock wave is found at its exit and its structure seems to be highly distorted.

For the three different kinds of pipe exit tested in the present study, Figure 11 shows the relationship between the peak value ($\Delta \mathbf{P}_m$) of the experimented impulse waves and

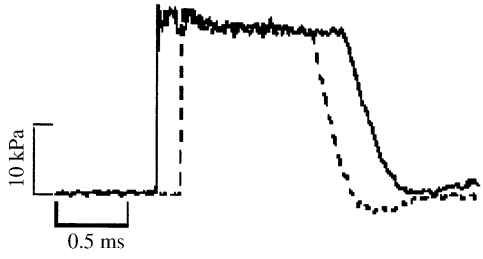

(a) **Straight pipe**

(b) **Right-angle smooth bend**

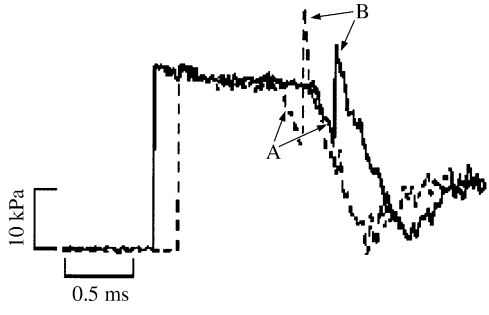

(c) **Right-angle miter bend**

Figure 7. Pressure signals at the measurement points ① and ②.

initial shock Mach number at $\theta = 0$, 45, and 90°, where the peak value of the impulse wave is normalized using atmospheric pressure $\mathbf{P}_a$. It is again noted that for the right-angle miter bend, the impulse wave has several distinct peak values. At $\theta = 0°$, the peak values of the impulse wave increases with the initial shock Mach number, regardless of the type of the pipe exit yielded. In the range of the present Mach number, the magnitude of the impulse wave seems to be the strongest in the straight pipe and the weakest in the right-angle miter bend. At $\theta = 45$ and 90°, it is found that the peak value of the impulse wave is the highest in the right-angle smooth bend and again the lowest in the right-angle miter bend. At $\theta = 90°$, the second peak of the impulse wave in the right-angle miter bend seems to be not strongly dependent on the initial Mach number, although the first peak of the impulse wave shows some weak dependency on the Mach number. In this case, the first peak of the impulse wave in the right-angle miter bend is nearly the same as the magnitude of the impulse wave of the straight pipe. The present results obviously show that the right-angle miter bend can reduce the magnitude of the impulse wave.

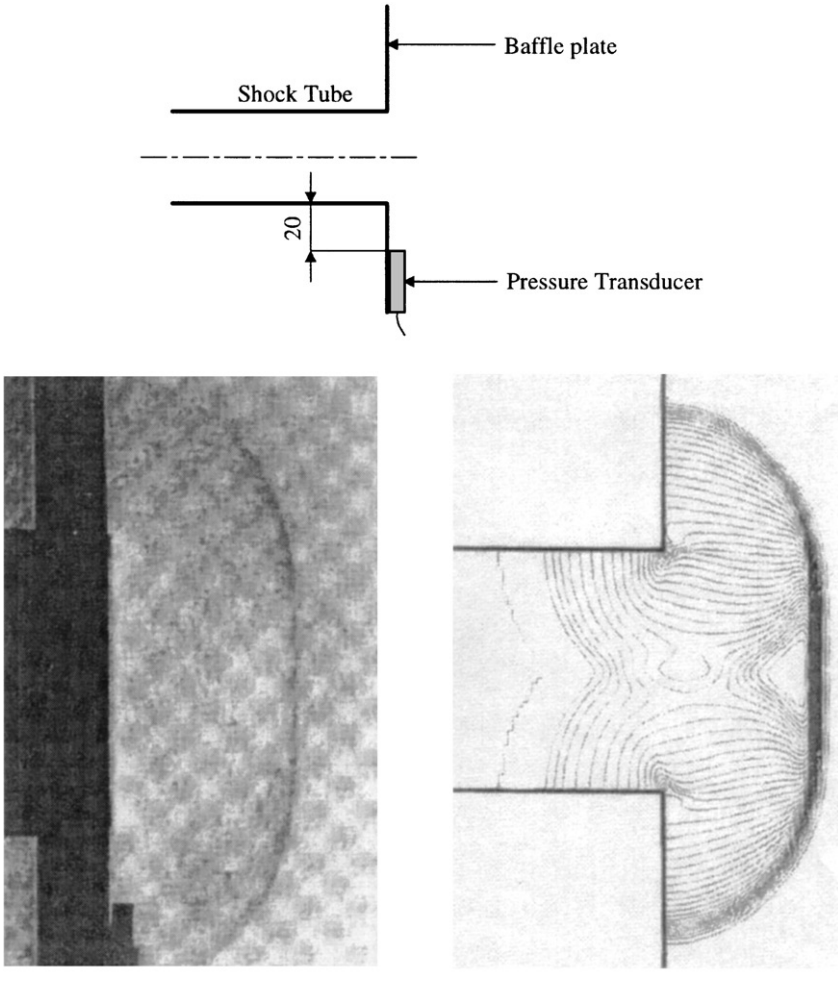

Figure 8. Schlieren picture and computed density contours showing the impulse wave at the exit of the straight pipe ($M = 1{\cdot}10$).

It is interesting to note that for both the straight pipe and the right-angle smooth bend, the impulse wave has a strong directivity toward $\theta = 0^\circ$, and this trend seems to be more significant in the straight pipe. However, in the right-angle miter bend, the impulse wave does not seem to be strongly dependent on θ; for all θ values tested, the magnitude of the impulse wave is nearly the same. It is, thus, reasonable to state that the right-angle miter bend can considerably reduce the directivity of the impulse wave toward the pipe axis.

For the right-angle smooth bend, Figure 12 shows the dependency of the impulse wave on θ and ψ. The magnitude of the impulse wave seems to be the strongest at $\theta = 0^\circ$ and the weakest at $\theta = -90^\circ$. For instance of $M = 1{\cdot}20$, the peak value of the impulse wave at $\theta = 0^\circ$ is about 16 per cent of atmospheric pressure, while at $\theta = -90^\circ$, it is about 5 per cent of atmospheric pressure.

In contrast to the impulse wave discharged from the exit of the right-angle smooth bend, it seems that the impulse wave for the right-angle miter bend does not strongly depend on

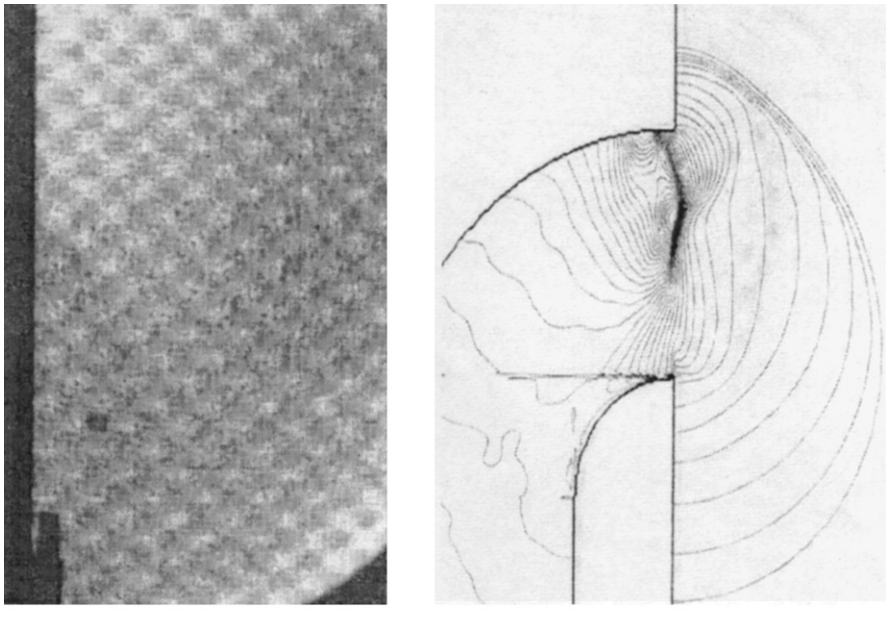

(a) **Schlieren picture (delay time=100μs)**

(b) **Computed density contours (t'=1.5540)**

Figure 9. Schlieren picture and computed density contours showing the impulse wave at the exit of the right-angle smooth bend ($M = 1{\cdot}10$).

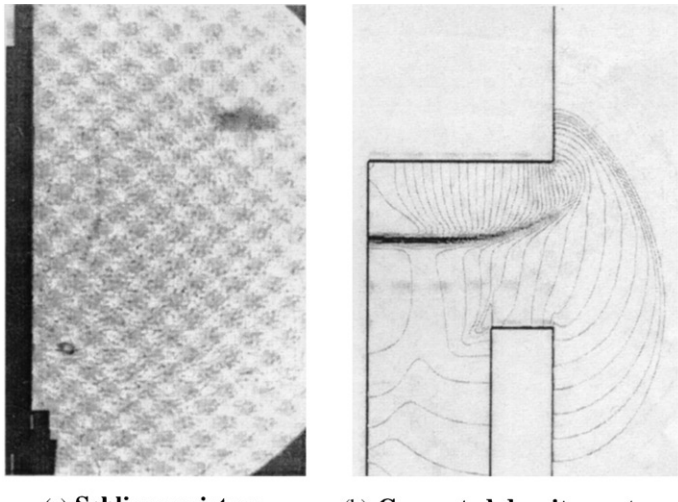

(a) **Schlieren picture (delay time=50μs)**

(b) **Computed density contours (t'=1.5540)**

Figure 10. Schlieren picture and computed density contours showing the impulse wave at the exit of the right-angle miter bend ($M = 1{\cdot}10$).

θ and ψ, as shown in Figure 13. The first peak of the impulse wave is nearly independent of both θ and ψ, while the second peak seems to be somewhat dependent on θ; being the strongest at $\theta = -45^\circ$. It can be also found from Figures 12 and 13 that for a given initial Mach number, the magnitude of the impulse wave is much lower in the right-angle

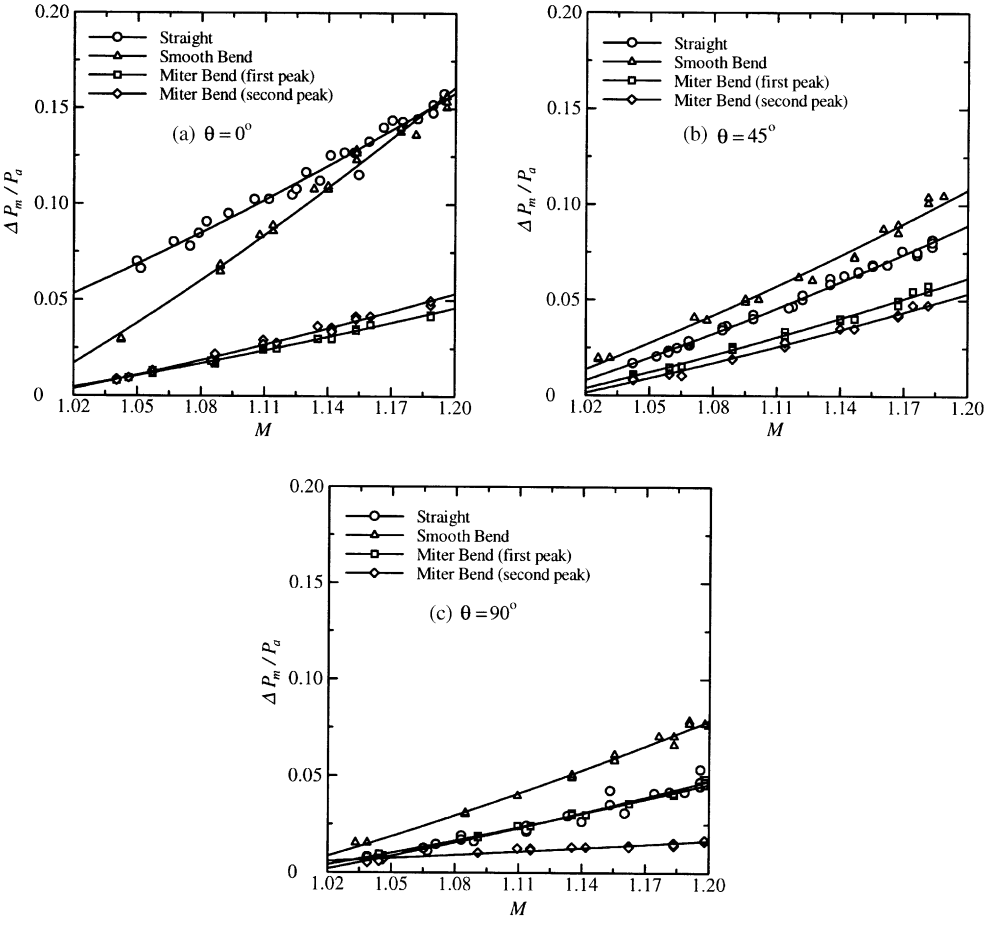

Figure 11. Peak pressure of impulse wave versus shock Mach number M.

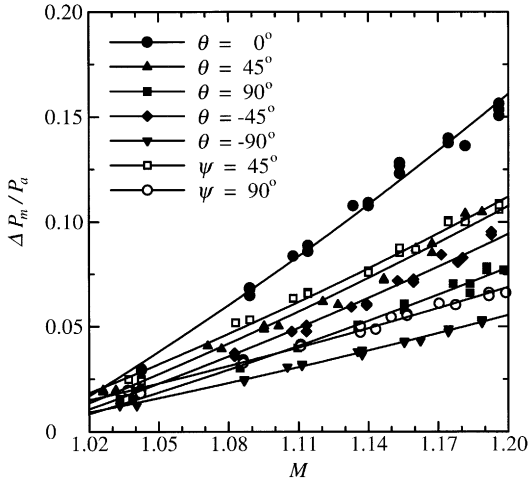

Figure 12. Dependency of the peak pressure of the impulse wave on θ and ψ (right-angle smooth bend).

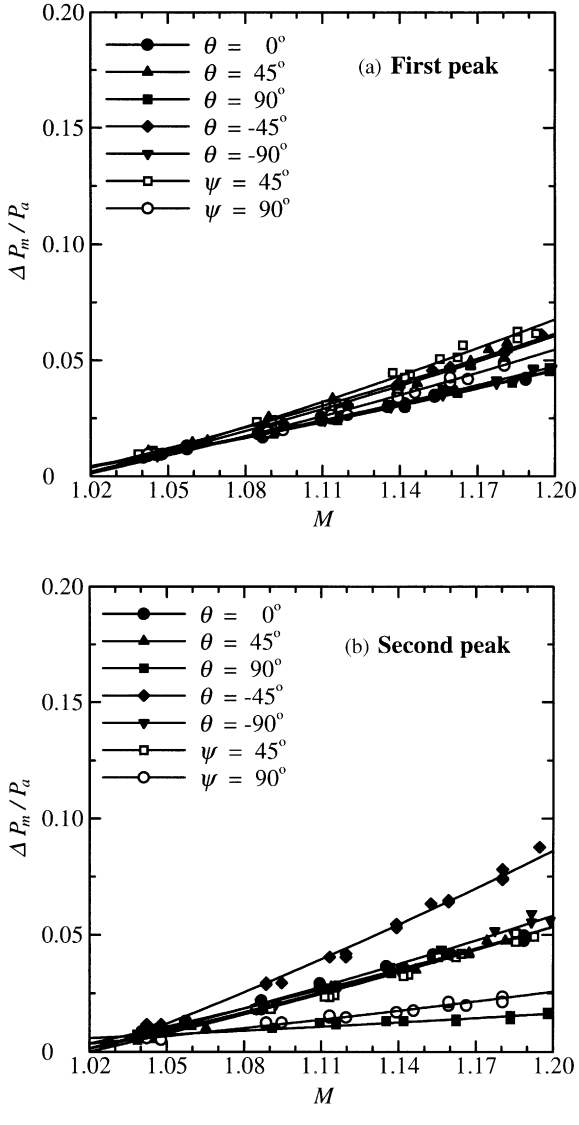

Figure 13. Dependency of the peak pressure of the impulse wave on θ and ψ (right-angle miter bend).

miter bend. This implies that the right-angle miter pipe bend can play the role of a passive control to reduce the magnitude of the impulse wave and its directivity toward the pipe axis.

5. CONCLUSIONS

The present study addresses experimental and computational work of the impulse wave discharged from the exit of two kinds of right-angle pipe bends, which are attached to the open end of a simple shock tube. The weak normal shock wave with its magnitude of Mach number from 1·02 to 1·20 is employed to obtain the impulse

wave propagating outside the exit of the pipe bends. The experimental data of the magnitude of the impulse wave and its propagation directivity are analyzed to characterize the impulse waves discharged from the exit of the pipe bends and compared with those discharged from a straight pipe. Computational analysis using the unsteady, inviscid, compressible equations is complemented to represent the major features of the impulse wave obtained from the shock tube experiments. Computational results well predict the experimented dynamic behaviors of the impulse wave. The results obtained show that the magnitude of the impulse wave increases with the initial shock Mach number, regardless of the type of the pipe bends yielded. A right-angle miter bend significantly reduces the magnitude of the impulse wave, as compared with the straight pipe and right-angle smooth pipe bend. For the straight pipe and right-angle smooth pipe bend, the impulse wave has a strong directivity toward the pipe axis, while the right-angle miter bend considerably reduces the directivity of the impulse wave toward the pipe axis. It is believed that the right-angle miter bend pipe can play the role of a passive control against the impulse wave.

REFERENCES

1. S. Raghunathan, H. D. Kim and T. Setoguchi 1998 *Progress in Aerospace Sciences* **34**, 1–44. Impulse noise and its control.
2. H. D. Kim, T. Setoguchi and K. Matsuo 1997 *JSME International Journal*, *Series B* **40**, 223–229. Reduction of impulsive noise caused by unsteady compression wave.
3. H. D. Kim and T. Setoguchi 1999 *Journal of Sound and Vibration* **226**, 1011–1028. Study of the discharge of weak shocks from an open end of a duct.
4. H. D. Kim, T. Setoguchi and H. Kashimura 2001 *Journal of Mechanical Engineering Sciences*, *IMechE Part C* **215**, 191–199. Augmentation of the magnitude of the impulsive wave discharging from a tube.
5. H. D. Kim and T. Setoguchi 2002 *Journal of Sound and Vibration* **256**, 197–211. Study of the impingement of impulse wave upon a flat plate.
6. N. Sekine, S. Matsumura, K. Aoki and K. Takayama 1989 *17th International Symposium on Shock Wave and Shock Tubes*, AIP Conference Proceedings of American Institute of Physics, New York, 671–676. Generation and propagation of shock waves in the exhaust pipe of a four cycle automobile engine.
7. J. A. C. Kentfield 1993 *Nonsteady*, *One-dimensional*, *Internal*, *Compressible Flows* (*Theory and Applications*). Oxford: Oxford University Press; chapter 7.
8. Maa Dah-you and LiPei-zi 1981 *Noise Control Engineering* **17**, 104–112. Pressure dependence of jet noise and silencing of blow-offs.
9. R. Klingel and Loffler 1983 *Proceedings of the Filtration Society*, *Filtration and Separation*, Vol. **20**, 205–208. Dust collection and cleaning efficiency of a pulse jet fabric filters, London.
10. K. Takayama and O. Onodera 1983 14*th International Symposium on Shock Wave and Shock Tubes*, Sydney, 205–212. Shock wave propagation past a circular cross sectional 90 degree bend.
11. K. Kage, K. Ishimatsu and H. Miyake 1994 3*rd Asian Symposium on Visualization, Chiba*, *Japan*, 271–276. Numerical visualization of propagating shock waves and induced flow in an elbow.
12. A. S. Sarigül 1999 *Journal of Sound and Vibration* **228**, 837–844. Sound attenuation characteristics of right-angle pipe bends.
13. H. C. Yee 1987 *NASA TM*-89464. Upwind and symmetric shock capturing schemes.
14. G. A. Sod 1977 *Journal of Fluid Mechanics* **83**, 785–794. A numerical study of a converging cylindrical shock.
15. H. Kashimura, H. D. Kim and T. Setoguchi 2000 *JSME Journal* **65**, 161–167. Emission of a propagating shock wave from an open end of a tube.
16. H. D. Kim, T. Setoguchi and Y. H. Kweon 1998 11*th International Symposium on Transport Phenomena*, *ISTP*-11, *Hsinchu*, *Taiwan*, 94–99. Studies on reflection of weak shock waves from an open end of a tube with baffle plate.

APPENDIX A: NOMENCLATURE

a	speed of sound
D	diameter
e	total energy per unit volume
M	shock wave Mach number
L	the median length of pipe bend
p	static pressure
r	radial distance
t	time
u	velocity component in the x direction
v	velocity component in the y direction
x	longitudinal distance in cylindrical co-ordinate
y	radial distance in cylindrical co-ordinate
γ	ratio of specific heats
ρ	density

SUPER/SUBSCRIPTS

a	atmospheric state
m	peak or maximum value
$*$	normal shock wave overpressure
$'$	non-dimensional quantity